

# *DFT modelling of the edge dislocation in 4H-SiC*

**J. Łażewski, P. T. Jochym, P. Piekarz,  
M. Sternik, K. Parlinski, J. Cholewiński,  
P. Dłużewski & S. Krukowski**

**Journal of Materials Science**

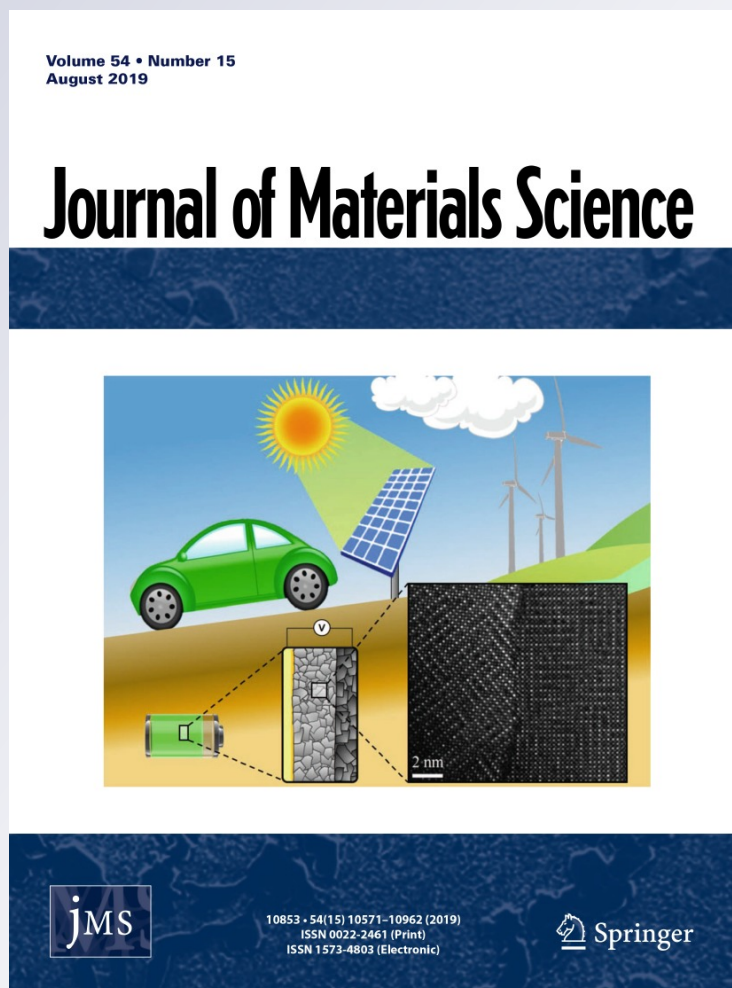
ISSN 0022-2461

Volume 54

Number 15

J Mater Sci (2019) 54:10737-10745








DOI 10.1007/s10853-019-03630-5



**Your article is published under the Creative Commons Attribution license which allows users to read, copy, distribute and make derivative works, as long as the author of the original work is cited. You may self-archive this article on your own website, an institutional repository or funder's repository and make it publicly available immediately.**



## DFT modelling of the edge dislocation in 4H-SiC

J. Łażewski<sup>1,\*</sup> , P. T. Jochym<sup>1</sup> , P. Piekarz<sup>1</sup> , M. Sternik<sup>1</sup> , K. Parlinski<sup>1</sup> ,  
J. Cholewiński<sup>2</sup>, P. Dłużewski<sup>2</sup> , and S. Krukowski<sup>3</sup> 

<sup>1</sup>Institute of Nuclear Physics, Polish Academy of Sciences, Radzikowskiego 152, 31-342 Kraków, Poland

<sup>2</sup>Institute of Fundamental Technological Research, Polish Academy of Sciences, Pawińskiego 5b, 02-106 Warsaw, Poland

<sup>3</sup>Institute of High Pressure Physics, Polish Academy of Sciences, Sokołowska 29/37, 01-142 Warsaw, Poland

Received: 8 January 2019

Accepted: 14 April 2019

Published online:

26 April 2019

© The Author(s) 2019

### ABSTRACT

We have presented ab initio study, based on density functional theory methods, of full-core edge dislocation impact on basic properties of 4H-SiC semiconductor. To enable calculations in periodic boundary conditions, we have proposed geometry with two dislocations with opposite Burgers vectors. For this geometry, which determines the distance between dislocations, we have estimated the creation energy per unit length of a single-edge dislocation. The radial distribution function has been used to assess the effect of the dislocations on the local crystal structure. The analysis of the electronic structure reveals mid-gap  $p$  states induced by broken atomic bonds in the dislocation core. The maps of charge distribution and electrostatic potential have been calculated, and the significant decrease in the electrostatic barriers in the vicinity of the dislocation cores has been quantified. The obtained results have been discussed in the light of previous findings and calculations based mainly on phenomenological models.

### Introduction

The silicon carbide (SiC), a wide band gap semiconductor, is a promising material for high-voltage and high-frequency nanoelectronic devices [1, 2]. Very good operational quality of SiC results from high values of breakdown voltage ( $\approx 10^6$  V/cm), high charge carrier mobility, high temperature stability and high thermal conductivity [3]. Additionally, this material has very good mechanical properties and resistance to radiation damage. Unfortunately, the electronic properties of epitaxial layers strongly depend on the material's quality. The presence of

intrinsic defects and impurities which arise during crystal growth process substantially limit applications of SiC.

Dislocations are the main crystal defects in SiC. They deteriorate the performance of high electric field devices such as Schottky and  $p$ - $n$  diodes [4, 5]. Two typical components of dislocations with the direction along [0001] are the screw and edge dislocations with Burgers vectors [0001] and  $\frac{1}{3}[2110]$ , respectively. The standard density of dislocations observed in the good quality 4H-SiC epilayers reaches  $10^3$  cm<sup>-2</sup> [6]. In the last decade, different

Address correspondence to E-mail: jan.lazewski@ifj.edu.pl

dislocation formation mechanisms were examined [7] and impact on important properties was studied. The electrical characteristics of 4H-SiC photodiodes reveal that the screw and edge dislocations reduce the breakdown voltage by 3.5% and 2%, respectively, and increase the leakage currents compared to systems without crystal defects [8]. Dislocations also influence transport properties of 4H-SiC by increasing recombination activity [9] and reducing the diffusion length in the material [10].

Various mechanisms are responsible for modifications of electronic structure in the presence of dislocations. In the dislocation core, the broken bonds give rise to acceptor levels within the band gap and make this region electrically active [11, 12]. Dislocations also act as trapping centres and sources for point defects [13]. In the vicinity of the core, the strain field may induce additional states located near the conduction band edge [14]. In epitaxially grown SiC, several gap levels have been detected using the deep-level transient spectroscopy (DLTS) and their connection with the intrinsic defects have been analysed [15, 16].

The structural properties of dislocations have been previously studied theoretically in very few materials using both empirical potentials [17] and ab initio methods based on the density functional theory (DFT) [18–21]. The DFT provides tools that allow one to study changes in electronic structure induced by dislocations [22]. Such computations revealed that the dislocation core in GaN induces deep-gap states [23, 24], which influence strongly the electronic and optical properties of this semiconductor [25]. The point defects such as vacancies and oxygen dopants can be easily trapped at the core of the edge dislocations providing additional mid-gap states [23, 26]. The influence of partial dislocations on the structural and electronic properties has been investigated in the pure SiC [27] and crystals doped with impurity atoms [28]. However, to our best knowledge, electronic properties of the full-edge dislocation have not been studied with ab initio methods yet.

In this work, we study the changes in the crystal structure and electronic properties of 4H-SiC induced by the edge dislocation. We analyse in detail the local lattice distortion by means of the radial distribution function (RDF)—the density of atoms in the spherical shell around given atom averaged over whole structure [29–31]. The calculations reveal significant redistribution of charges and electrostatic potential in

the region of the dislocation core. The electronic states located in the insulating gap, arising from the dislocation core atoms, show a very weak dispersion in the perfect correlation with the distribution of charges in the distorted region. Estimated minimal electrostatic barriers for ideal and distorted systems throw a new light on the decrease in the breakdown voltage in the defected 4H-SiC crystal.

## Methods

All presented calculations have been executed with the Vienna Ab initio Simulation Package (VASP) [32, 33] using the full-potential projector augmented-wave method [34, 35] with the generalised-gradient approximation (GGA) to the exchange-correlation functional in the PBE form [36–38]. The following valence base configurations have been included: Si  $3s^23p^2$  and C  $2s^22p^2$ . The integration over the  $\mathbf{k}$ -point space has been performed over the  $2 \times 2 \times 2$  Monkhorst-Pack mesh [39], and the energy cut-off for the plane waves expansion was equal to 500 eV.

The supercell has been prepared using following procedure. In the first step, a perfect 4H-SiC lattice region containing several SiC unit cells in each direction was created. Next, using different slip planes, two mutually opposite edge dislocations were inserted into the perfect lattice. To this aim, the following analytic formulas expressing the relation between the lattice displacements  $\mathbf{u}$  and displaced atoms coordinates  $\mathbf{x}$  have been adopted [40–44]:

$$\begin{aligned} u_1 &= \frac{b_1}{2\pi} \left[ \text{atan2}(x_2, x_1) + \frac{x_1 x_2}{2(1-\nu)(x_1^2 + x_2^2)} \right] \\ u_2 &= \frac{b_1}{8\pi(\nu-1)} \left[ (1-2\nu) \ln \frac{x_1^2 + x_2^2}{r_o^2} + \frac{x_1^2 - x_2^2}{x_1^2 + x_2^2} \right] \\ u_3 &= \frac{b_3}{2\pi} \text{atan2}(x_2, x_1), \end{aligned} \quad (1)$$

where  $b_1$  and  $b_3$  denote the Burgers vector edge and screw components, respectively,  $\nu$  is the Poisson ratio and  $r_o$  normalises the vertical shift in the dislocation cores and  $x_i$  are the components of the position vector in the distorted lattice. The atan2 function is a commonly used version of arctan function which observes quadrant where the  $(x_1, x_2)$  point is located. In our case, because Burgers vector is coaxial with  $x_1$  axis and  $b_2 = 0$ , the general equation system (Eq. 1) reduces to the first two rows. The analytic formulas

(Eq. 1) define lattice distortion  $\mathbf{u}$  as a function of displaced atoms coordinates  $\mathbf{x}$ :  $\mathbf{u} = f(\mathbf{x})$ . However, for any practical use, the distortion as a function of initial coordinates  $\mathbf{X}$  is needed. To obtain this function, a nonlinear equation  $\mathbf{u} = f(\mathbf{X} + \mathbf{u})$  must be solved. The solution can be obtained numerically by means of standard iterative methods. In the present work, the modified Powell's hybrid method [45] has been used, as implemented in Visual Editor of Crystal Defects (VECDs) [46]. At each iteration step, the standard Newton iteration was performed first. If the solution leaves so-called trusted region of the values, then linear combinations of the Newton iteration and conjugate gradient method were employed. A simultaneous insertion of two edge dislocations by slips over the same slip plane corresponds to the superposition of the analytic formulas discussed above. The different positions of dislocation cores resulted from the different lengths of slips applied to each of the dislocations. After the insertion of dislocations into the lattice, a supercell containing two dislocations has been cut out from the region to provide periodic boundary conditions.

The supercell obtained in this way needs relaxation; therefore, the structures of ideal and defected crystals have been fully optimised (with respect to lattice parameters, stresses, and atomic positions) in the supercells consisting of  $8 \times 6 \times 1$  primitive unit cells, containing 384 and 346 atoms, which correspond to crystal volumes of  $25\text{\AA} \times 19\text{\AA} \times 10\text{\AA}$  and  $22\text{\AA} \times 19\text{\AA} \times 10\text{\AA}$ , respectively. We have used the conjugate gradient technique with the energy convergence criteria set at  $10^{-8}$  eV and  $10^{-5}$  eV for the electronic and ionic iterations, respectively.

## Results

### Crystal structure

The pure 4H-SiC crystal structure has been reproduced correctly with the lattice constants  $a = 3.095\text{\AA}$  and  $c = 10.132\text{\AA}$ , which are very close to experimental values that amount to  $3.073\text{\AA}$  and  $10.053\text{\AA}$ , respectively. To fulfil the periodic boundary conditions, we consider two full-core edge dislocations with opposite Burgers vectors  $\frac{1}{3}[\bar{2}110]$  and  $\frac{1}{3}[2\bar{1}\bar{1}0]$ , inserted into the system using VECDs package [46]. The procedure involves removal of 38 selected atoms (19 SiC molecules) changing the total number of

atoms in the system. This has been taken into account in all comparisons to the ideal structure. Despite decreased atom count in the distorted structure, the relaxed crystal volume noticeably increases (by about 1%) due to the local destruction of hexagonal close-packed structure. However, since the supercell is big enough, the elongation of the average nearest neighbour bond is below 0.5% in comparison with its length in the ideal system.

The creation energy per unit length of a single-edge dislocation has been calculated using the following formula [24]:

$$e = (E - E'_0)/2c, \quad (2)$$

where  $E$  is the energy of the system with a pair of dislocations (346 atoms) and  $E'_0$  is the ground state energy of the undisturbed system normalised to the same number of formula units. For the relative distance between the cores equal to  $6.73\text{\AA}$ , we have obtained  $e = 2.17\text{ eV/\AA}$  per supercell. Additionally, it has been found—in agreement with [42]—that due to attractive force between dislocations of opposite sign, they easily annihilate. Otherwise, if they repel each other, they would create a stable grid in the periodic boundary conditions, which does not happen. It proves that the Peierls energy barrier between two states of dislocation core at adjacent lattice nodes along the common glide plane is very low. Therefore, to prevent the annihilation of defects during optimisation process, we have trapped both dislocations by pinning their cores at different glide planes.

The optimised 4H-SiC structure with two edge dislocations is presented in Fig. 1. The positions of dislocation lines have been marked by atoms distinguished by different colour. Carrying out crystal structure relaxation, without any symmetry constraints, we have found that it tends to self-recover—reconstructing as much as possible of pure 4H-SiC coordinations and so gathering most of the disorder to the dislocation cores (mostly I in Fig. 1).

To analyse the influence of the dislocation on its nearest neighbourhood, the RDF for the dislocation dipole has been calculated and analysed. In Fig. 2, one can immediately notice that the introduction of the edge dislocation disturbs hexagonal close-packed structure which results in slight increase in the nearest neighbour and next nearest neighbour distances visible as shift from pure 4H-SiC positions (dashed lines). We discovered that each coordination shell can be fitted with a two-component function

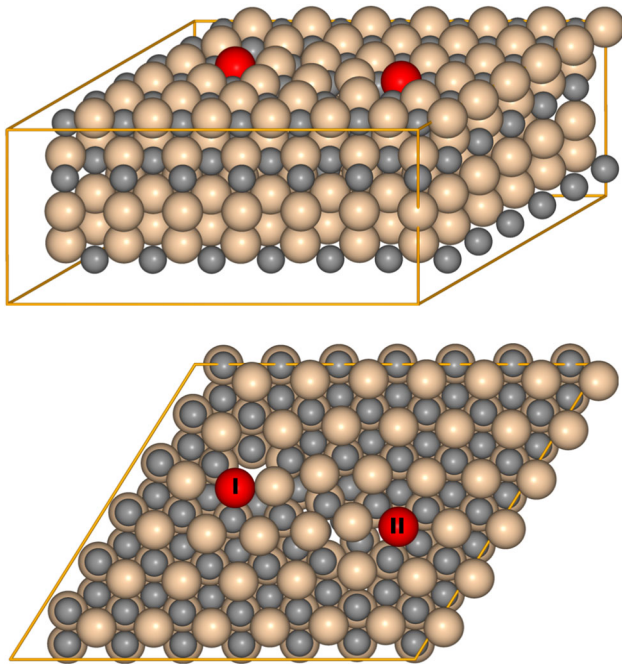


**Figure 1** Off-bottom (upper panel) and top (lower panel) view of the optimised crystal structure of 4H-SiC with two full-core edge dislocations. Both dislocation edges (I and II) have been distinguished by coloured atoms.

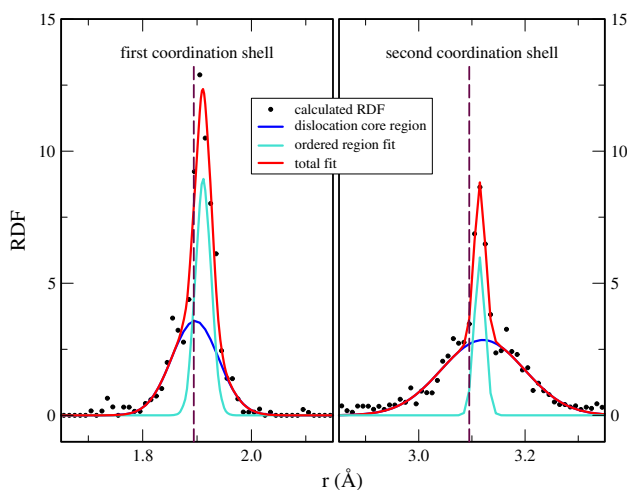


**Figure 2** RDF of the first- (left panel) and the second-coordination shell (right panel) for the edge dislocation dipole in 4H-SiC (points), fitted with the two-component Gaussian (solid lines). The dashed lines mark positions of the coordination shells for the ideal 4H-SiC system.

(two Gaussian lines with parameters collected in Table 1): the central part with small width and the rest reproducing broad tails behaviour. In particular,

**Table 1** The parameters of Gaussian functions (positions and FWHM) and calculated peak areas of two-component fit of RDF presented in Fig. 2. *u* and *d* parts corresponds to the undisturbed and distorted regions, respectively

	Nearest neighbour		Next nearest neighbour	
	<i>u</i>	<i>d</i>	<i>u</i>	<i>d</i>
Position	1.911	1.896	3.115	3.121
Area	0.321	0.387	0.154	0.560
FWHM	0.034	0.101	0.024	0.185

this is clearly visible for the second-coordination shell (right panel in Fig. 2).

We have found that the components with a narrow and broad full width at half maximum (FWHM) correspond to the undistorted part of the crystal and disordered dislocation core, respectively. For bigger supercells with smaller densities of dislocations, the latter component will remain mostly unchanged, while the former one will increase and converge towards a delta function. Due to interaction between dislocations, RDF picture depends on their mutual distance. Thus, the ratio of both mentioned contributions can be different, while the two-component character of coordination shell peaks remains unchanged.

## Band structure

Next, we analyse the influence of edge dislocations on the band structure of the 4H-SiC. The general observation is that the positions of the main bands in the electron density of states (eDOS) remain mostly unchanged (see Fig. 3). The characteristic peaks in the valence and conduction bands of the ideal structure become broadened and smeared out in the system with dislocations. The strongest changes are found inside the energy gap of the pure 4H-SiC crystal,<sup>1</sup> where additional localised states appear. One can find sharp deep states delivered by atoms with broken nearest neighbours bonds and broadened shallow bands close to the top of the valence band and the bottom of the conduction band. The presence of shallow bands effectively reduces the magnitude of the insulating gap. The states located in the range

<sup>1</sup> The theoretical gap  $E_g = 2.3$  eV is smaller than the measured value (3.2 eV) due to well-known gap underestimation problem in the LDA/GGA approaches.

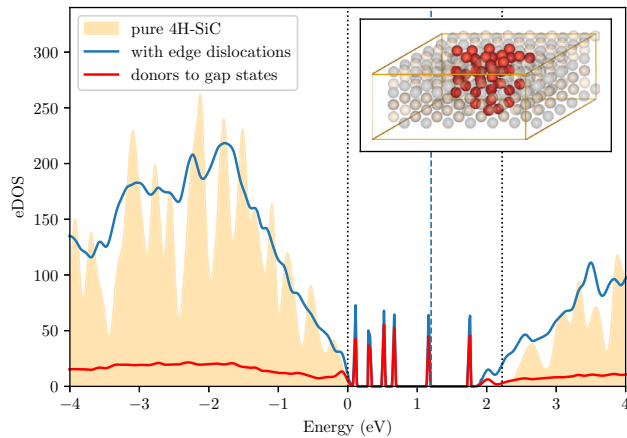


**Figure 3** The electronic density of states (eDOS) calculated for pure 4H-SiC (filled contours) compared with results obtained for the distorted system (blue line), and contribution to eDOS of 40 dominant donors to the gap states (red line). Fermi energy level has been marked with dashed blue line and the energy gap limits of the undisturbed system by the black dotted lines. Inset—positions of the dominant 40 donors to the gap states (red spheres).

~0.2–0.6 eV below the conduction band have also been found in the SiC systems with the stacking faults [47–49] and Shockley partial dislocations [27]. The latter may also induce the occupied states about 0.4 eV above the valence band. Furthermore, the defects generated by relaxations around the dislocation may also introduce defect states into the gap [49–51].

All deep states are very narrow which indicates their weak dispersion in the Brillouin zone and localised character. It is possible to trace the distribution of individual states in the whole spectrum, as well as to identify atoms which contribute to the eDOS in a particular energy range. In the inset of Fig. 3, we have marked 40 atoms which have the largest contribution to the mid-gap states, constituting 70% of the eDOS in the gap. We have found that the mid-gap states are mainly localised on atoms from the strongly distorted region (see Fig. 1), i.e. from the dislocation core and the area between the cores. These atoms’ bonding geometry is significantly disturbed. The contribution to gap eDOS from atoms situated outside this area quickly diminishes with distance. The detailed analysis has led to the conclusion that also the partial eDOS projected onto the *spd* states has been modified. For the conduction band, where in the perfect 4H-SiC *d* states dominate, as well as for the localised states inside the gap, the

main contribution for distorted system stems from *p* states.

### Electric charge distribution

The charge density is a well-defined, primary quantity in the DFT. Fig. 4a presents the charge distribution around edge dislocations. In particular, one can see the elongated structures with a very low charge density (outlined with dotted line in Fig. 4a) in the

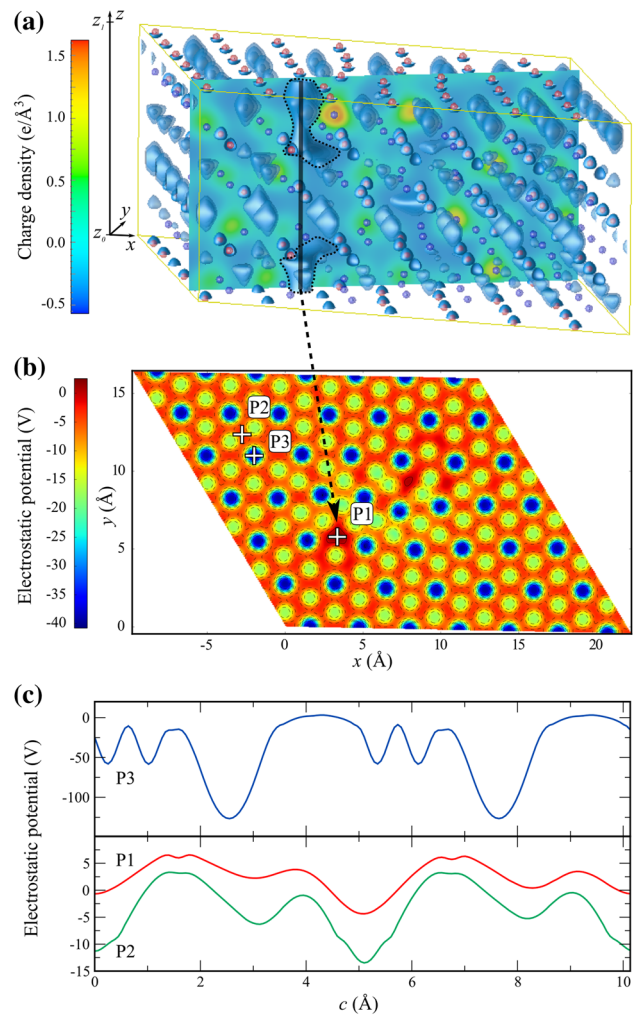


**Figure 4** **a** Off-bottom view of charge distribution in distorted system. The slice plane crosses through both edge dislocations cores. The increased carrier density areas (bright, well-defined yellow clouds) visible on cross section stem from the deep orbitals electrons and pseudo-cores of atomic nuclei and have no connection with the dislocations. **b** Top view of electrostatic potential derived from charge distribution averaged along *c* direction. **c** The electrostatic potential along *c*-axis direction in P1 (dislocation core), P2 (between atoms in the ordered, undisturbed region) and P3 (atomic chain) places marked in (b).

slice plane crossing both dislocation cores. On the other hand, the neighbouring atoms visible in Fig. 4a have increased density of carriers connected with broken interatomic bonds. The effect is more pronounced for the dislocation I, marked with the thick solid line in the figure. The electrostatic potential derived from the charge distribution and averaged over  $c$  direction is presented in the top-view projection (Fig. 4b). The decreased charge density regions exhibit lowered energy barriers which allow for easier flow of the carriers. Again, the effect is much stronger for the dislocation I with the bigger disorder around its edge. Additionally, panel (c) shows the electrostatic potential along the  $c$  direction in three different locations of distorted system. Its periodicity reflects ABCB stacking in the 4H-SiC structure. In agreement with the intuition, electric charges encounter the highest barriers along the atomic chain (curve P3 in Fig. 4c) and the lowest barriers through the dislocation core (curve P1 - note different vertical scales on upper and lower panels).

To quantify the influence of dislocations on the energy barriers for the electron transport along  $c$ -axis, we have analysed the local electrostatic potential in the crystal. We have taken into account that the path over minimal barriers does not always follow a straight line parallel to the  $c$  direction. Therefore, for each pair of positions:  $p_0 = (x, y, z_0)$  and  $p_1 = (x, y, z_1)$ —where  $z_0$  is at the bottom of the periodic unit, while  $z_1$  is at its top (see Fig. 4a)—we have derived a minimal energy path and the barrier height for this path from  $p_0$  to  $p_1$ . The calculation used the basin-filling segmentation algorithm [52] with bisection search for minimal limiting energy level. The results indicate substantial lowering of the barrier in the vicinity of the dislocation cores denoted by P1 in Fig. 4b. The calculated difference between the minimal barrier height in the non-distorted area and in the vicinity of the dislocation core is 0.8 V. This value is much lower than the differences in barrier heights presented in Fig. 4c due to the nonlinear character of the minimal barrier path. The calculated energy barriers are obtained with zero voltage bias and as such are not sufficient to determine quantitatively the charge transport properties of the material but are an important step towards full understanding of charge carriers' behaviour.

On the basis of the presented results, the following mechanism of the insulating properties weakening

and the breakdown voltage decreasing in the 4H-SiC monocrystal may be proposed. In the edge dislocation core, part of interatomic bonds is broken causing the creation of deep states inside the semiconductor gap. Additionally, crystal distortions modify the atomic potential facilitating the shallow states formation and simultaneously narrowing the forbidden gap. Finally, the elongated regions of the reduced charge density with flat electrostatic potential are formed along a dislocation cores. The lack of barriers inside so-created tunnels, in connection with additional empty states in the energy gap, may enhance carrier flow through the distorted areas, significantly influencing decrease in the breakdown voltage. This scenario provides the plausible explanation of the current-voltage characteristics of the 4H-SiC avalanche photodiodes, which show a measurable decrease in the breakdown voltage and increase in leakage currents due to a single-edge dislocation [8]. Our analysis of the mid-gap levels also enables a better understanding of a pronounced impact of dislocations on the carrier lifetime [9] and diffusion length [10] and can be helpful in interpreting the DLTS measurements [15, 16]. Moreover, similarly to other strongly defected systems [53], the changes in the electronic structure may be related to observable effects in the lattice dynamical and optical properties of SiC [54].

## Conclusions

In this work, we have successfully modelled a pair of edge dislocations using ab initio methods. Our results are consistent with experimental findings concerning small but noticeable lattice constants elongation, semiconductor energy gap narrowing and electrostatic barriers reduction. Furthermore, with atomic-scale resolution, we have explained foregoing processes. We have shown that (i) the crystal structure is strongly disturbed in the small vicinity of the dislocation core, (ii) additional energy levels occurring in the energy gap belong to the atoms with broken bonds occupying the core neighbourhood, (iii) existence of spatial tunnels, with atoms delivering localised states to the band structure on its sides, significantly decreases electrostatic barriers and should be considered as one of the primary factors responsible for experimentally observed reduction in breakdown voltage.



The presented research demonstrates the possibility of modelling the extended crystal defects within the DFT approach and periodic boundary conditions. So far, most of the published results employed the models with empirical potentials, focusing on the structural or elastic properties of dislocations. The ab initio approach allows us to study the microscopic properties of the lattice and electronic degrees of freedom on an equal footing. Therefore, it was possible to identify the atoms from the distorted region of the crystal, with the largest contribution to the mid-gap electronic states. Since DFT provides the information about the charge density and potential at each point of space, we could analyse its distribution in the defected crystal and study potential barriers within the dislocation core. These results help to better understand the changes in electronic properties and transport properties induced by extended defects. Such study was performed for the first time and may have a strong impact on further research of edge dislocations and other crystal defects.

The presented work could be extended in different directions. Using larger cells would be beneficial for better understanding of size effects and the dependence of structural and electronic properties on the distance between dislocations. Increasing the supercell size will require extensive computations; however, it may provide relevant information about the interaction between dislocations, allow to determine their formation energies and in perspective explain the mechanism of micropipe creation. Another important step is to study magnetic properties of the localised states induced by the broken bonds. Such local magnetic moments, generated by vacancies, were previously studied experimentally and theoretically in the SiC crystals. The presence of dislocations also modify elastic properties of materials. The total-energy DFT method is a perfect tool to study the changes in elastic constants of defected crystals, and it will be the aim of our future research.

## Acknowledgements

This work was partially supported by the SICMAT Project financed under the European Funds for Regional Development (Contract No. UDA-POIG.01.03.01-14-155/09).

**Open Access** This article is distributed under the terms of the Creative Commons Attribution 4.0 International License (<http://creativecommons.org/licenses/by/4.0/>), which permits unrestricted use, distribution, and reproduction in any medium, provided you give appropriate credit to the original author(s) and the source, provide a link to the Creative Commons license, and indicate if changes were made.

## References

- [1] Zolper JC, Skowronski M (2005) Advances in silicon carbide electronics. *MRS Bull* 30:273–278
- [2] Choyke WJ, Matsunami H, Pensl G (eds) (2004) Silicon carbide: recent major advances. Springer, Berlin
- [3] Bechstedt F, Käckell P (1995) Heterocrystalline structures: new types of superlattices? *Phys Rev Lett* 75:2180–2183
- [4] Neudeck PG (2000) Electrical impact of SiC structural crystal defects on high electric field devices. *Mater Sci Forum* 338–342:1161–1166
- [5] Singh R (2006) Reliability and performance limitations in SiC power devices. *Microelectron Reliab* 46:713–730
- [6] Chen Y, Zhang N, Huang XR, Black DR, Dudley M (2008) Studies of the distribution of elementary threading screw dislocations in 4H silicon carbide wafer. *Mater Sci Forum* 600–603:301–304
- [7] Ishikawa Y, Sugawara Y, Saitoh H, Danno K, Suzuki H, Bessho T, Kawai Y, Shibata N (2012) Microscopic structure of stepwise threading dislocation in 4H-SiC substrate. *Jpn J Appl Phys* 51:041301
- [8] Berechman RA, Skowronski M, Soloviev S, Sandvik P (2010) Electrical characterization of 4H-SiC avalanche photodiodes containing threading edge and screw dislocations. *J Appl Phys* 107:114504
- [9] Maximenko S, Soloviev S, Cherednichenko D, Sudarshan T (2004) Electron-beam-induced current observed for dislocations in diffused 4H-SiC P-N diodes. *Appl Phys Lett* 84:1576–1578
- [10] Maximenko SI, Freitas JA, Myers-Ward RL, Lew K-K, VanMil BL, Eddy CR, Gaskill DK, Muzykov PG, Sudarshan TS (2010) Effect of threading screw and edge dislocations on transport properties of 4H-SiC homoepitaxial layers. *J Appl Phys* 108:013708
- [11] Shockley W (1953) Some predicted effects of temperature gradients on diffusion in crystals. *Phys Rev* 91:1563–1564
- [12] Pearson GL, Read WT, Morin FJ (1954) Dislocations in plastically deformed germanium. *Phys Rev* 93:666–667

- [13] Schröter W, Kronewitz J, Gnauert U, Riedel F, Seibt M (1995) Bandlike and localized states at extended defects in silicon. *Phys Rev B* 52:13726–13729
- [14] Celli V, Gold A, Thomson R (1962) Electronic states on dislocations in semiconductors. *Phys Rev Lett* 8:96–97
- [15] Danno K, Nakamura D, Kimoto T (2007) Investigation of carrier lifetime in 4H-SiC epilayers and lifetime control by electron irradiation. *Appl Phys Lett* 90:202109
- [16] Sasaki S, Kawahara K, Feng G, Alfieri G, Kimoto T (2011) Major deep levels with the same microstructures observed in n-type 4H-SiC and 6H-SiC. *J Appl Phys* 109:013705
- [17] Duesbery MS, Joos B, Michel DJ (1991) Dislocation core studies in empirical silicon models. *Phys Rev B* 43:5143–5146
- [18] Bigger JRK, McInnes DA, Sutton AP, Payne MC, Stich I, King-Smith RD, Bird DM, Clarke LJ (1992) Atomic and electronic structures of the 90 degree partial dislocation in silicon. *Phys Rev Lett* 69:2224–2227
- [19] Arias TA, Joannopoulos JD (1994) Ab initio theory of dislocation interactions: From close-range spontaneous annihilation to the long-range continuum limit. *Phys Rev Lett* 73:680–683
- [20] Blase X, Lin K, Canning A, Louie SG, Chrzan DC (2000) Structure and energy of the 90 degree partial dislocation in diamond: a combined ab initio and elasticity theory analysis. *Phys Rev Lett* 84:5780–5783
- [21] Cai W, Bulatov VV, Chang J, Li J, Yip S (2001) Anisotropic elastic interactions of a periodic dislocation array. *Phys Rev Lett* 86:5727–5730
- [22] Kontsevoi OY, Gornostyrev YN, Mryasov ON, Freeman AJ, Katsnelson MI, Trefilov AV (2001) Electron localization on dislocations in metals: real-space first-principles calculations. *Phys Rev B* 64:134103
- [23] Lee SM, Belkhir MA, Zhu XY, Lee YH, Hwang YG, Frauenheim T (2000) Electronic structures of GaN edge dislocations. *Phys Rev B* 61:16033–16039
- [24] Lymperakis L, Neugebauer J, Albrecht M, Remmele T, Strunk HP (2004) Strain induced deep electronic states around threading dislocations in GaN. *Phys Rev Lett* 93:196401
- [25] You JH, Johnson HT (2007) Effect of threading edge dislocations on the photoluminescence spectra for n-type wurtzite GaN. *Phys Rev B* 76:115336
- [26] Elsner J, Jones R, Heggie MI, Sitch PK, Haugk M, Frauenheim T, Öberg S, Briddon PR (1998) Deep acceptors trapped at threading-edge dislocations in GaN. *Phys Rev B* 58:12571–12574
- [27] Blumenau AT, Fall CJ, Jones R, Öberg S, Frauenheim T, Briddon PR (2003) Structure and motion of basal dislocations in silicon carbide. *Phys Rev B* 68:174108
- [28] Bernardini F, Colombo L (2005) Interaction of doping impurities with the 30 degree partial dislocations in SiC: an ab initio investigation. *Phys Rev B* 72:085215
- [29] Chandler D (1987) Introduction to modern statistical mechanics. Oxford University Press, New York
- [30] Hansen J-P, McDonald IR (2013) Theory of simple liquids, 4th edn. Elsevier, Amsterdam
- [31] Kittel C (1986) Introduction to solid state physics, 6th edn. Wiley, New York
- [32] Kresse G, Furthmüller J (1996) Efficiency of ab-initio total energy calculations for metals and semiconductors using a plane-wave basis set. *Comput Mater Sci* 6:15–50
- [33] Kresse G, Furthmüller J (1996) Efficient iterative schemes for ab initio total-energy calculations using a plane-wave basis set. *Phys Rev B* 54:11169–11186
- [34] Blöchl PE (1994) Projector augmented-wave method. *Phys Rev B* 50:17953–17979
- [35] Kresse G, Joubert D (1999) From ultrasoft pseudopotentials to the projector augmented-wave method. *Phys Rev B* 59:1758–1775
- [36] Perdew JP, Chevary JA, Vosko SH, Jackson KA, Pederson MR, Singh DJ, Fiolhais C (1992) Atoms, molecules, solids, and surfaces: applications of the generalized gradient approximation for exchange and correlation. *Phys Rev B* 46:6671–6687
- [37] Perdew JP, Chevary JA, Vosko SH, Jackson KA, Pederson MR, Singh DJ, Fiolhais C (1993) Erratum: Atoms, molecules, solids, and surfaces: applications of the generalized gradient approximation for exchange and correlation. *Phys Rev B* 48:4978–4978
- [38] Perdew JP, Burke K, Ernzerhof M (1996) Generalized gradient approximation made simple. *Phys Rev Lett* 77:3865–3868
- [39] Monkhorst HJ, Pack JD (1976) Special points for Brillouin-zone integrations. *Phys Rev B* 13:5188–5192
- [40] Love AEH (2013) A treatise on the mathematical theory of elasticity, 4th edn. Cambridge University Press, Cambridge
- [41] deWit R (1973) Theory of disclinations: IV. Straight disclinations. *J Res Natl Bur Stand Sect Phys Chem* 77A:607–658
- [42] Hirth JP, Lothe J (1982) Theory of dislocations, 2nd edn. Wiley, New York
- [43] Read WT Jr (1953) Dislocations in crystals. McGraw-Hill, New York
- [44] Cholewiński J, Maździarz M, Jurczak G, Dłużewski P (2014) Dislocation core reconstruction based on finite deformation approach and its application to 4H-SiC crystal. *Int J Multiscale Comput Eng* 12:411–421
- [45] Galassi M (2009) GNU scientific library: reference manual, 3rd edn. Network Theory, Bristol

- [46] Dłużewski P, Cholewiński J. VECDS software. <http://sourceforge.net/projects/vecds/>. Accessed 29 July 2016
- [47] Miao MS, Limpijumnong S, Lambrecht WRL (2001) Stacking fault band structure in 4H-SiC and its impact on electronic devices. *Appl Phys Lett* 79:4360–4362
- [48] Iwata H, Lindefelt U, Öberg S, Briddon PR (2001) Localized electronic states around stacking faults in silicon carbide. *Phys Rev B* 65:033203
- [49] Lindefelt U, Iwata H, Öberg S, Briddon PR (2003) Stacking faults in 3 C -, 4 H -, and 6 H - SiC polytypes investigated by an ab initio supercell method. *Phys Rev B* 67(15):155204
- [50] Deretzis I, Camarda M, La Via F, La Magna A (2012) Electron backscattering from stacking faults in SiC by means of ab initio quantum transport calculations. *Phys Rev B* 85(23):235310
- [51] Xi J, Liu B, Zhang Y, Weber WJ (2016) Ab initio study of point defects near stacking faults in 3C-SiC. *Comput Mater Sci* 123:131–138
- [52] Pal NR, Pal SK (1993) A review on image segmentation techniques. *Pattern Recognit* 26:1277–1294
- [53] Wdowik UD, Piekarz P, Parlinski K, Oleś AM, Korecki J (2013) Strong effects of cation vacancies on the electronic and dynamical properties of FeO. *Phys Rev B* 87:121106
- [54] Talwar DN (2015) Probing optical, phonon, thermal and defect properties of 3C-SiC/Si (001). *Diam Relat Mater* 52:1–10

**Publisher's Note** Springer Nature remains neutral with regard to jurisdictional claims in published maps and institutional affiliations.